Seasonal cycle of N_2O: Analysis of data

Xun Jiang,[1] Wai Lim Ku,[2,3] Run-Lie Shia,[2] Qinbin Li,[4] James W. Elkins,[5] Ronald G. Prinn,[6] and Yuk L. Yung[2]

Received 13 January 2006; revised 22 August 2006; accepted 18 September 2006; published 26 January 2007.

[1] We carried out a systematic study of the seasonal cycle and its latitudinal variation in the nitrous oxide (N_2O) data collected by National Oceanic and Atmospheric Administration–Global Monitoring Division (NOAA-GMD) and the Advanced Global Atmospheric Gases Experiment (AGAGE). In order to confirm the weak seasonal signal in the observations, we applied the multitaper method for the spectrum analysis and studied the stations with significant seasonal cycle. In addition, the measurement errors must be small compared with the seasonal cycle. The N_2O seasonal cycles from seven stations satisfied these criteria and were analyzed in detail. The stations are Alert (82°N, 62°W), Barrow (71°N, 157°W), Mace Head (53°N, 10°W), Cape Kumukahi (19°N, 155°W), Cape Matatula (14°S, 171°W), Cape Grim (41°S, 145°E) and South Pole (90°S, 102°W). The amplitude (peak to peak) of the seasonal cycle of N_2O varies from 0.29 ppb (parts-per-billion by mole fraction in dry air) at the South Pole to 1.15 ppb at Alert. The month at which the seasonal cycle is at a minimum varies monotonically from April (South Pole) to September (Alert). The seasonal cycle in the Northern Hemisphere shows the influence of the stratosphere; the seasonal cycle of N_2O in the Southern Hemisphere suggests greater influence from surface sources. Preliminary estimates are obtained for the magnitude of the seasonally varying sources needed to account for the observations.

Citation: Jiang, X., W. L. Ku, R.-L. Shia, Q. Li, J. W. Elkins, R. G. Prinn, and Y. L. Yung (2007), Seasonal cycle of N_2O: Analysis of data, *Global Biogeochem. Cycles*, *21*, GB1006, doi:10.1029/2006GB002691.

1. Introduction

[2] The sources of nitrous oxide (N_2O) are the microbes in nitrification and denitrification processes as well as anthropogenic activities [*Stein and Yung*, 2003]. As the nitrogen cycle has been perturbed by human activities [*McElroy et al.* 1977], the concentration of N_2O in the terrestrial atmosphere has been increasing from the pre–industrial revolution value of about 270 ppb (parts-per-billion by mole fraction in dry air or nmol/mol) to the present value of 320 ppb [*Battle et al.*, 1996; *Thompson et al.*, 2004].

[3] The sink of N_2O is mainly photolysis in the stratosphere with a smaller contribution from reaction with O (^1D), resulting in a very long lifetime of about 125 years for atmospheric N_2O [*Minschwaner et al.*, 1993; *Volk et al.*, 1997; *McLinden et al.*, 2003; *Morgan et al.*, 2004]. This is the primary reason why the seasonal cycle signal in the troposphere is so small and previously clearly detectable only at Tasmania in the AGAGE network [*Prinn et al.*, 2000]. However, the long accumulation of high-quality data has finally made it possible to study the seasonal cycle. The seasonal cycle of N_2O in the stratosphere is caused primarily by the seasonally varying Brewer-Dobson circulation [*Morgan et al.*, 2004; *Nevison et al.*, 2004]. The seasonal cycle in the troposphere is caused partly by the mixing of N_2O-poor stratospheric air with tropospheric air in the spring of each hemisphere [*Levin et al.*, 2002; *Liao et al.*, 2004; *Nevison et al.*, 2004]. In addition to dynamical transport, there is a seasonal cycle arising from the surface sources of N_2O. There is considerable uncertainty in the magnitude, distribution and the temporal pattern of the various natural and anthropogenic sources of N_2O [*Bouwman et al.*, 1995]. Investigation of the seasonal cycle and its latitudinal variation of the N_2O should shed light on its sources, sinks, and transport processes. In this paper, we will carry out an analysis of surface N_2O observations.

[4] The data and the method of analysis are described in section 2. The main results are presented in section 3, followed by conclusions in section 4.

2. Data and Methodology

[5] We obtained the N_2O observation from four sources: National Oceanic and Atmospheric Administration–Global

[1]Division of Geological and Planetary Sciences, California Institute of Technology, Pasadena, California, USA.
[2]Division of Geological and Planetary Sciences, California Institute of Technology, Pasadena, California, USA.
[3]Now at Department of Physics, Chinese University of Hong Kong, Shatin, Hong Kong.
[4]Jet Propulsion Laboratory, California Institute of Technology, Pasadena, California, USA.
[5]Earth System Research Laboratory, Global Monitoring Division, NOAA, Boulder, Colorado, USA.
[6]Center for Global Change Science, Department of Earth, Atmospheric, and Planetary Science, Massachusetts Institute of Technology, Cambridge, Massachusetts, USA.

0886-6236/07/2006GB002691

Table 1. Locations of Stations and Length of Records in All Measurement Programs[a]

Measurement Program	Station Name	Latitude	Longitude	Time
NOAA flask	Alert (ALT)	82°N	62°W	2/1988–12/1995; 12/1994–8/2002
	Barrow (BRW)	71°N	157°W	9/1977–12/1995; 12/1994–10/2002
	Niwot Ridge (NWR)	40°N	106°W	8/1977–12/1995; 1/1995–10/2002
	Cape Kumukahi (KUM)	19°N	155°W	11/1995–10/2002
	Mauna Loa (MLO)	19°N	156°W	9/1977–12/1995; 1/1995–10/2002
	Cape Matatula (SMO)	14°S	171°W	10/1977–12/1995; 11/1994–10/2002
	Cape Grim (CGO)	40°S	145°E	5/1991–12/1995; 2/1995–10/2002
	South Pole (SPO)	90°S	102°W	5/1977–12/1995; 3/1995–2/2002
CATS	Barrow (BRW)	71°N	157°W	6/1998–12/2004
	Niwot Ridge (NWR)	40°N	106°W	1/2001–11/2004
	Mauna Loa (MLO)	19°N	156°W	12/1999–12/2004
	Cape Matatula (SMO)	14°S	171°W	1/1999–12/2004
	South Pole (SPO)	90°S	102°W	1/1998–12/2004
AGAGE	Mace Head (MHD)	53°N	10°W	3/1994–3/2003
	Trinidad Head	45°N	124°W	10/1995–3/2003
	Ragged Point	13°N	59°W	7/1996–3/2003
	Cape Matatula (SMO)	14°S	171°W	9/1996–3/2003
	Cape Grim (CGO)	40°S	145°E	9/1993–3/2003
RITS	Barrow (BRW)	71°N	157°W	9/1987–2/1999
	Niwot Ridge (NWR)	40°N	106°W	2/1990–8/2001
	Mauna Loa (MLO)	19°N	156°W	6/1987–4/2000
	Cape Matatula (SMO)	14°S	171°W	9/1987–4/2000
	South Pole (SPO)	90°S	102°W	1/1989–11/2000

[a]The data are available from the following websites: NOAA flask: ftp://ftp.cmdl.noaa.gov/hats/n2o/flasks/; CATS: ftp://ftp.cmdl.noaa.gov/hats/n2o/insituGCs/CATS/global/insitu_global_N2O; AGAGE: http://cdiac.ornl.gov/ftp/ale_gage_Agage/AGAGE/gc-md/monthly/; RITS: ftp://ftp.cmdl.noaa.gov/hats/n2o/insituGCs/RITS/.

Monitoring Division (NOAA-GMD) Halocarbons and other Atmospheric Trace Species Flask Program (NOAA flask), NOAA-GMD Chromatograph for Atmosphere Trace Species (CATS), NOAA-GMD Radiatively Important Trace Species (RITS), and the Advanced Global Atmospheric Gases Experiment (AGAGE) Global Trace Gas Monitoring Network. The NOAA flask data are divided into two separate data sets, before and after 1996. The RITS data are from 1988 to 1999 and the CATS data are from 1999 to 2004 [*Thompson et al.*, 2004]. The AGAGE data are divided into three sets, ALE(1978–1986), GAGE(1985–1996), and AGAGE(1993–2003), respectively [*Prinn et al.*, 2000]. Since there are many gaps in the RITS and NOAA flask pre-1996 data, we will mainly focus on the NOAA flask post-1996, AGAGE 93-03, and CATS data. The locations of the stations in each of the measurement programs and the length of the records are listed in Table 1.

[6] NOAA-GMD N_2O measurements have evolved since 1977, improving with new gas chromatographic techniques and more precise detectors. The early 1977–1995 flasks (pre-1996 data) were measured using a nitrogen carrier gas and electron capture detector coupled to a gas chromatograph (ECD-GC). Water vapor was not removed in those samples because of concern of affecting the mixing ratios of other trace gases measured (CFCs) at the parts-per-trillion. The correction varied from 0% for dry stations to almost 3% for wet stations. There was a slight CO_2 effect on the column used at the time, which amounted to 0.1 ppb of N_2O per 1 ppm in the difference in CO_2 of the air sample minus that of the calibration tank. The typical corrections were from 0.1 to 2 ppb. The precisions of the pre-1996 flask data were about 1.5%. The advantage of that system was that the calibration tanks were changed only about 6 times, so there were fewer shifts due to calibration uncertainties in the final assignment of mixing ratio. Flasks in a pair are collected at each station each week whenever possible. The frequency of in situ measurements is once an hour. The NOAA flask post-1996 data, RITS, and CATS system dried the air before sample injection, so there is no water correction. These systems have no CO_2 correction because they use an argon-methane carrier gas (P-5, 5% CH_4 in Ar), and a long Porapak Q column. The CO_2 effect is checked periodically and is undetectable in the post-1996 data and in situ measurements. The individual precisions of each analysis system depended on the station location and time. The individual precisions are given in the individual data files located at ftp://ftp.cmdl.noaa.gov/hats/n_2o. The precisions of the CATS system vary from 0.2 to 1.2 ppb, being highest at Niwot Ridge. The absolute calibration error is estimated at 1%, but the assignment of a calibration tank mixing ratio is between 0.2 and 0.4 ppb consistency with gravimetrically prepared standards from GMD. The mean offset of one method versus the next method is better than 1 ppb. By separating the N_2O detection techniques, we have eliminated the problem of offsets to any new calibration and comparing sets with the same experimental operating parameters.

[7] Since we are trying to extract a very weak signal from noisy data, we need an objective criterion to ensure reliable detection. Following *Liao et al.* [2004], we applied the multitaper method (MTM) [*Ghil et al.*, 2002] to establish the existence of the N_2O seasonal cycle. MTM reduces the variance of spectral estimates by using a small set of tapers. Tapers are the specific solution to an appropriate variational problem. Averaging over the ensemble of spectra obtained by this procedure yields a better and more stable estimate than single-taper methods. The parameters of the MTM

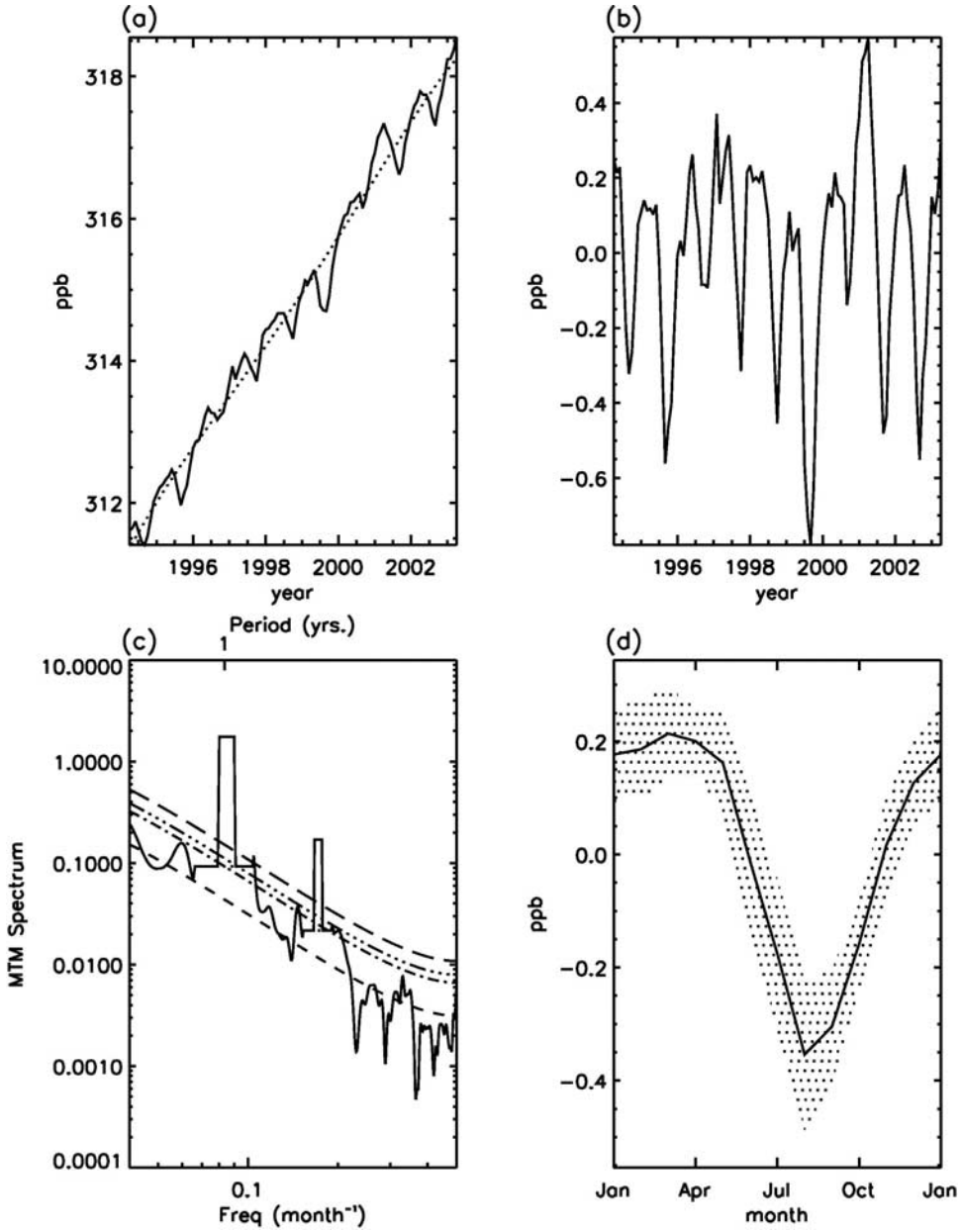

Figure 1. Analysis of N_2O AGAGE data at Mace Head (53°N, 10°W). (a) Raw data (solid line) and fourth-order polynomial trend (dotted line). (b) Detrended data. (c) Estimate of power spectrum by multitaper method. The dashed lines represent the median, 10%, 5%, and 1% significance level. (d) Seasonal cycle of N_2O derived from monthly weighted means (solid line). Shaded area represents the estimated error, $\sigma = \sqrt{\sigma_Z^2 + \sigma_S^2}$, for the seasonal cycle.

analysis must be chosen to give a good compromise between the required frequency resolution for resolving distinct signals and the benefit of reduced variance; we chose the resolution to be 2 and the number of tapers to be 3 [*Ghil et al.*, 2002; *Liao et al.*, 2004]. Longer data sets permit the use of a larger number of tapers. The criterion we chose was that the seasonal cycle must be smaller than 1% significance level. A small numerical value of the significance level denotes a high statistical confidence.

[8] We used the above-mentioned three data sets, NOAA flask post-1996, AGAGE 93-03, and CATS, to calculate the N_2O seasonal cycle. First, we used a fourth-order polynomial to fit the trend in the monthly mean data. We compared the difference between the fourth-order polynomial and the fifth-order polynomial, and found no significant difference. Therefore we used the fourth-order polynomial in all subsequent work. After detrending the data by the fourth-order polynomial fitting and removed the mean value, we

Table 2. Separation of Data Sets Into Two Groups According To Whether the Seasonal Cycle is Below or Above 1% Significance Level[a]

Data	Below 1%	Above 1%
NOAA flask pre-1996	Alert (0.267)	Niwot Ridge
	Barrow (0.160)	Cape Matatula
	Mauna Loa (0.174)	South Pole
	Cape Grim (0.289)	
NOAA flask post-1996	Alert (0.062)*	Niwot Ridge
	Barrow (0.060)	Mauna Loa
	Cape Kumakahi (0.047)*	Cape Matatula
		Niwot Ridge
		South Pole
ALE 78–86		Mace Head
		Trinidad Head
	None	Ragged Point
		Cape Matatula
		Cape Grim
GAGE 85–96		Mace Head
		Trinidad Head
	None	Ragged Point
		Cape Matatula
		Cape Grim
AGAGE 93-03	Mace Head (0.022)*	Trinidad Head
	Cape Matatula (0.033)*	Ragged Point
	Cape Grim (0.024)*	
CATS	Barrow (0.004)*	Mauna Loa
	South Pole (0.007)*	Cape Matatula
		Niwot Ridge
RITS	Barrow (0.070)	Mauna Loa
	Niwot Ridge (0.182)	Cape Matatula
	South Pole (0.066)	

[a]The standard deviations of measurement errors are given in brackets by $\frac{1}{N}\sqrt{\sum_{j=1}^{N}\sigma_j^2}$. Units are ppb. Seven stations marked by asterisks are selected for detailed study.

obtain N_2O anomaly, C_{ij}, where i is the index for the month (i ranges from 1 to 12), and j is the index for the year (j ranges from 1 to N). The units for C_{ij} are ppb. The seasonal cycle is computed by

$$S_i = \sum_{j=1}^{N} \left(C_{ij}/\sigma_{ij}^2\right)\sigma_t^2, \tag{1}$$

where S_i is the residual monthly concentration of N_2O, σ_{ij} is the standard deviation of measurement error for the ith month and the jth year, and $\sigma_t^2 = \left[\sum_{j=1}^{N} 1/\sigma_{ij}^2\right]^{-1}$. The standard deviation, σ, for each of the 12 months is then determined by $\sigma = \sqrt{\sigma_Z^2 + \sigma_S^2}$, where σ_Z^2 and σ_S^2 are the variances for the multimeasurement errors and for the seasonal values in each month. The units for C_{ij}, S_i, and σ are ppb. The details of the error estimate are deferred to Appendix A.

[9] As a demonstration of our methodology, we show the AGAGE data (solid line) at Mace Head (53°N, 10°W) from 1994 to 2003 and fourth-order polynomial trend (dotted line) in Figure 1a. The residual between the raw data and the trend is shown in Figure 1b. The MTM power spectrum of the detrended data is shown in Figure 1c. There is a strong seasonal cycle (1 year) at <1% significance level. The seasonal cycle of N_2O computed using (1) is shown in Figure 1d. Shaded area in Figure 1d represents the estimated error σ for the seasonal cycle. We also analyzed the Mace Head N_2O data as functions of time by an empirical model consisting of Legendre functions and harmonic (cos, sin) functions [*Prinn et al.*, 2000] and obtained a similar seasonal cycle.

3. Results and Discussion

[10] The statistical significance of the seasonal cycle for the N_2O from 40 data sets listed in Table 1 is summarized in Table 2. The data sets are separated into two groups according to whether the seasonal cycle is below or above 1% significance level. The data sets with seasonal cycle above 1% significance level have relatively large measurement errors or short data length. There are 15 data sets with seasonal cycles that have smaller than 1% significance level. The standard deviations of measurement errors for these 15 data sets are given in brackets. The NOAA flask pre-1996 data have relatively larger measurement errors than NOAA flask post-1996, AGAGE 93-03, CATS, and RITS data. Also, when we have more than one data set for the same location, we use the data with smaller measurement errors. After applying this criterion, seven stations, marked by asterisks in Table 2, are selected for detailed study. These include NOAA flask post-1996, AGAGE 93-03, and CATS. The stations with larger measurement errors will be discussed in Appendix B.

[11] The seasonal cycles of these seven data sets are shown in Figure 1d and Figures 2a–2f. In the Northern Hemisphere (NH), there are three stations. The first two stations, Alert (ALT) and Barrow (BRW), have positive values in winter and negative values in summer. The maxima are about 0.4 ppb in March and January, respectively. The minima are about −0.7 ppb in September. The third station in the NH is Mace Head (MHD). The maximum for MHD is 0.21 ppb in March. The minimum is −0.35 ppb in August. The MHD results are in excellent agreement with those in Figure 1a of *Nevison et al.* [2004]. If we take the average of the three NH stations, the result is consistent with Figure 4 of *Liao et al.* [2004], which used pre-1996 NOAA flask data. The pre-1996 data was noisy, because of greater instrumental imprecision, and CO_2 and H_2O corrections that had to be applied to the original data.

[12] In the tropics, there are two stations with significant seasonal cycles, Cape Kumukahi (KUM) and Cape Matatula (SMO). KUM has a maximum of 0.19 ppb in February, and a minimum of −0.3 ppb in June. SMO has a maximum of 0.3 ppb in January. SMO has a minimum of −0.24 ppb in June.

[13] In the Southern Hemisphere (SH), there are two stations with significant seasonal cycles, Cape Grim (CGO) and South Pole (SPO). They both have positive values before February and after August. SPO has a maximum of 0.2 ppb in November and a minimum value about −0.11 ppb in April. CGO has a maximum of 0.2 ppb in December, while the minimum is −0.2 ppb in May. The CGO results are in good agreement with those shown in Figure 1c of *Nevison et al.* [2004].

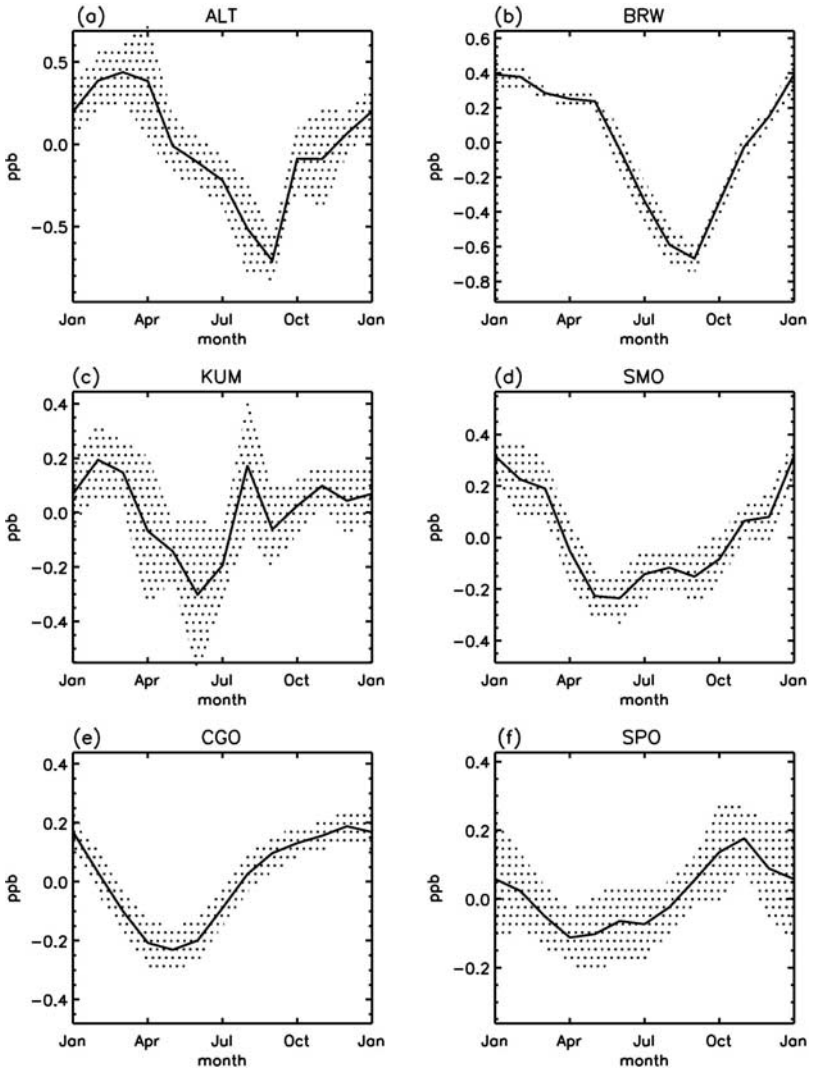

Figure 2. Same as Figure 1d for AGAGE, CATS, and NOAA flask data. The solid line is the seasonal cycle. Shaded area represents the estimated error of the seasonal cycle. (a) NOAA flask, Alert (82°N, 62°W). (b) CATS, Barrow (71°N, 157°W). (c) NOAA flask, Cape Kumukahi (19°N, 155°W). (d) AGAGE, Cape Matatula (14°S, 171°W). (e) AGAGE, Cape Grim (41°S, 145°E). (f) CATS, South Pole (90°S, 102°W).

[14] Details for the seasonal amplitude and months for maximum and minimum are summarized in Table 3. There is a latitudinal monotonic decrease in the peak-to-peak amplitude from 1.15 ppb at Alert to 0.29 ppb at the South Pole. There appears to be a phase shift of the month of the minimum from April at the South Pole to September at Alert. For the maximum, the phase shifts from November at the South Pole to March at Alert. These results are clearly seen in Figures 3 and 4.

[15] The fourth-order polynomial N_2O trends for the seven stations are shown in Figure 5a. The slopes are approximately 0.76, 0.83, 0.76, 0.84, 0.80, 0.79, 0.85 ppb/yr for the seven stations from north to south. The cosine weighted averages for NH, SH and whole planet are 0.81, 0.79, and 0.80 ppb/yr, respectively. The N_2O trends are due to the anthropogenic forcing, and are approximately parallel for the seven stations. The N_2O trends in 2000, 2001, and 2002 are shown in Figure 5b. The cosine weighted mean for the N_2O in the NH are 315.58, 316.44, and 317.31 ppb for year 2000, 2001, and 2002.

Table 3. Summary of the Peak-To-Peak Amplitude in ppb, Month of Maximum, and Month of Minimum in the Seasonal Cycles Shown in Figure 1d and Figures 2a–2f

Station	Amplitude	Maximum Month	Minimum Month
Alert	1.15	March	Sep
Barrow	1.06	Jan	Sep
Mace Head	0.57	March	Aug
Cape Kumukahi	0.50	Feb	June
Cape Matatula	0.55	Jan	June
Cape Grim	0.42	Dec	May
South Pole	0.29	Nov	April

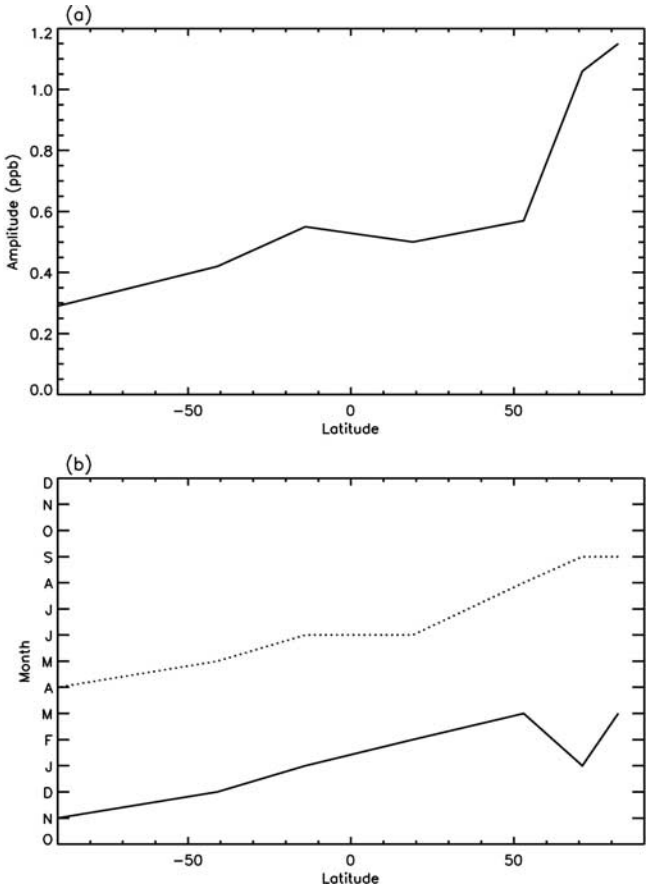

Figure 3. (a) N_2O seasonal cycle amplitudes for the seven stations. (b) Latitude distribution of maximum (solid line) and minimum (dotted line) month in the N_2O seasonal cycle.

The cosine weighted mean for the N_2O in the SH are 314.95, 315.76, and 316.44 ppb for the three years. The cosine weighted mean for the global N_2O are 315.29, 316.12, and 316.91 ppb for the three years. Averaged over the three years, the N_2O concentration in the NH is higher than that in the SH by 0.73 ppb. Implications for the sources of N_2O are as follows.

[16] The Global Emission Inventory Activities (GEIA) [*Bouwman et al.*, 1995] provides a detailed global N_2O emission inventory. The data are the total emission in one year. There are nine types of sources in the inventory, including soil, ocean, post–forest clearing soil, animal excreta, industry, fossil fuel burning, biofuel burning, agriculture, and biomass burning. A hemispheric breakdown of several sources of N_2O is listed in Table 4. We sort the sources in four groups, each plotted by latitude in Figure 6. The two major sources are soil (Figure 6a) and ocean (Figure 6b), which emit 7.532 and 3.598 Tg N/yr respectively. Anthropogenic sources, including animal excreta, industry, fossil fuel burning, biofuel burning, and agriculture, are added together in Figure 6c. The total emission for the anthropogenic sources is 1.971 Tg N/yr. The post–forest clearing soil and biomass burning are summed in Figure 6d, with total emission of 0.452 Tg N/yr. The ocean source, shown in Figure 6b, is mainly in the SH. In the tropics, the N_2O sources are soil, post–forest clearing soil, and biomass burning. To investigate the surface source difference between the two hemispheres, we use a two-box model by *Cicerone* [1989]. We assume the exchange time between hemispheres is 1.5 years. The rates of N_2O loss due to stratospheric processes in both hemispheres are 1/125 yr^{-1}. No soil sink is included. To account for the 0.73 ppb N_2O interhemispheric difference observed in the atmosphere, the difference of N_2O sources between NH and SH is about

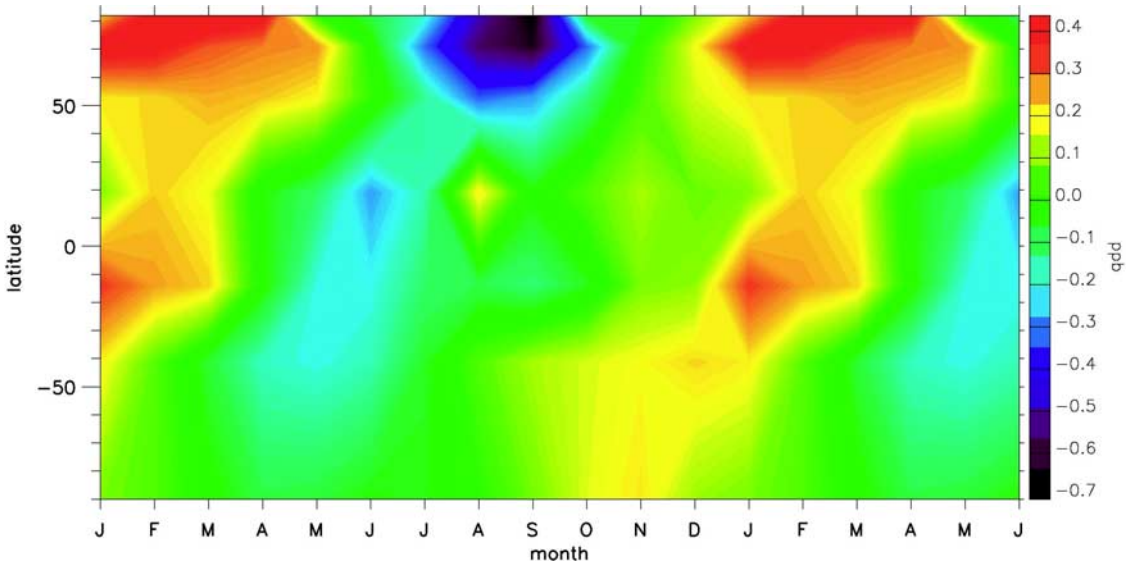

Figure 4. Seasonal cycle from the data of seven stations: Alert, Barrow, Cape Kumukahi, Mace Head, Cape Matatula, Cape Grim, and South Pole. The data for the first 6 months of the year are repeated after December.

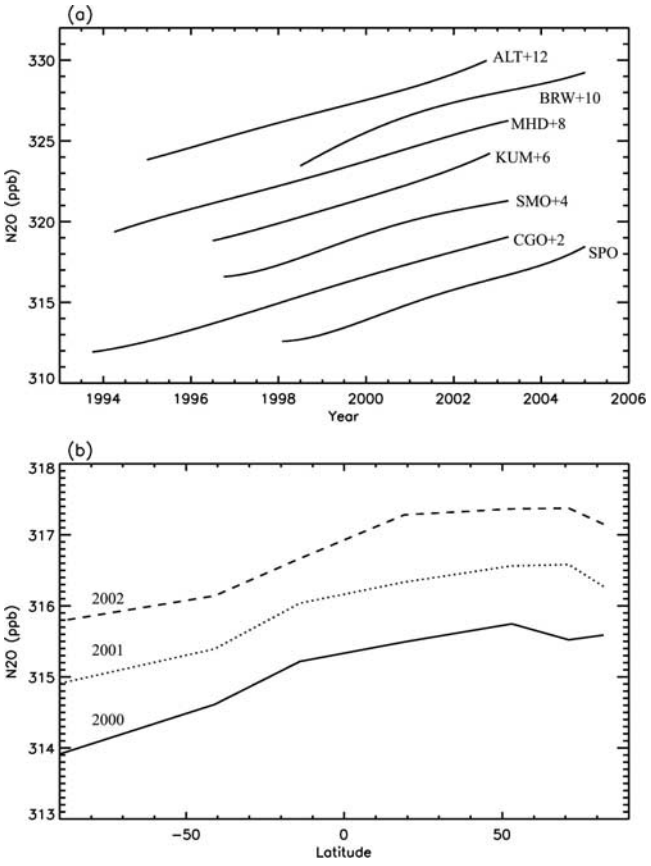

Figure 5. (a) Fourth-order polynomial N_2O trend for the seven stations. For visualizations, the N_2O trends for Alert, Barrow, Mace Head, Cape Kumukahi, Cape Matatula, and Cape Grim have been shifted upward by 12, 10, 8, 6, 4, and 2 ppb, respectively. (b) N_2O variation with latitude in 2000 (solid line), 2001 (dotted line), and 2002 (dashed line).

4.7 Tg N/yr, which is similar to the results from *Prinn et al.* [1990]. It is larger than the GEIA estimated interhemispheric emission difference 2.657 Tg N/yr in Table 4.

[17] The trends in N_2O data shown in Figure 5 represent annually averaged values. There are reasons to expect that the trends are seasonally dependent. In other words, the increase of N_2O may result in a change in its seasonal pattern. To investigate the seasonally varying N_2O trend, we use the data at BRW, MHD, SMO, and CGO, which have no gaps and have smaller errors than those at ALT, KUM, and SPO. For illustration, the N_2O data at MHD are shown in Figure 7 for June (crosses) and October (diamonds). The slope is determined by minimizing the chi-square. The N_2O trend is higher in October than in June for MHD. The N_2O trends for all months are determined in this way and are shown for the aforementioned four stations in Figure 8, along with error bars. For stations BRW and MHD, which are in the NH, the N_2O trends have large seasonal cycles. The peak-to-peak amplitudes are about 0.15 ppb/yr for both stations. In the SH, the seasonal cycle for the N_2O trend is large at SMO with a peak-to-peak amplitude about 0.15 ppb/yr. The seasonal cycle for the N_2O trend is small at CGO with amplitude of 0.06 ppb/yr.

[18] As pointed out by previous studies [*Levin et al.*, 2002; *Liao et al.*, 2004; *Nevison et al.*, 2004], the N_2O seasonal cycle in the NH may be related to the circulation in the stratosphere. The N_2O seasonal cycle in the SH may be related to the seasonal cycle in the ocean source [*Nevison et al.*, 2005]. The cause of N_2O seasonal cycle in the tropics is currently unidentified. We provide here a simple estimate that relates the seasonal cycle in N_2O concentration to its source using a heuristic model. The model describes the time evolution of the concentration of N_2O, which has a linear sink and a source [*Camp et al.*, 2001],

$$\frac{dC(t)}{dt} = -\frac{C(t)}{\tau} + S(t) \tag{2a}$$

$$S(t) = (A_0 + A_1 \sin(\omega t))/\tau, \tag{2b}$$

where $C(t)$ is the concentration of N_2O, τ is the lifetime of the N_2O, and $S(t)$ consists of a steady state term and a sinusoidally varying term, ω is the frequency for the annual cycle. The solution to equation (2a) is

$$C(t) = \left[C(0) - A_0 + \frac{A_1 \sin\phi}{\sqrt{1+\omega^2\tau^2}}\right] e^{-t/\tau} + A_0 + \frac{A_1 \sin(\omega t - \phi)}{\sqrt{1+\omega^2\tau^2}}, \tag{3}$$

where $C(0)$ is the initial concentration of N_2O. Because the mean lifetime of N_2O is about 125 yrs, we have $\omega\tau \gg 1$. Then we get $\phi = \arctan(\omega\tau) \approx \pi/2$ and $\sqrt{1+\omega^2\tau^2} \approx \omega\tau$. Now the nontransient solution for equation (2a) can be written as

$$C(t) \approx A_0 + \frac{A_1 \sin(\omega t - \phi)}{\sqrt{1+\omega^2\tau^2}} \approx A_0 + \frac{A_1 \sin(\omega t - \pi/2)}{\omega\tau} = A_0 - \frac{A_1 \cos(\omega t)}{\omega\tau}. \tag{4}$$

From equations (2b) and (4), we note that the oscillatory parts of $S(t)$ and $C(t)$ are related by $\omega = 2\pi/T$, where T = 1 year. This result can be used to estimate the relative importance of A_0 and A_1 in the N_2O source.

[19] Figure 3a suggests that the seasonal amplitude (peak to peak) consists of a roughly uniform global value of 0.5 ppb. The higher NH high latitude value of 1 ppb is

Table 4. Sources of N_2O[a]

Source	NH	SH	Global
Soil	4.601	2.931	7.532
Ocean	1.546	2.052	3.598
Anthropogenic sources	1.701	0.270	1.971
Post-forest clearing soil + biomass burning	0.257	0.195	0.452
Total sources	8.105	5.448	13.553

[a]Units are Tg N/yr. Anthropogenic sources include animal excreta, industry, fossil fuel burning, biofuel burning, and agriculture. The latitudinal distributions of the sources are plotted in Figure 6.

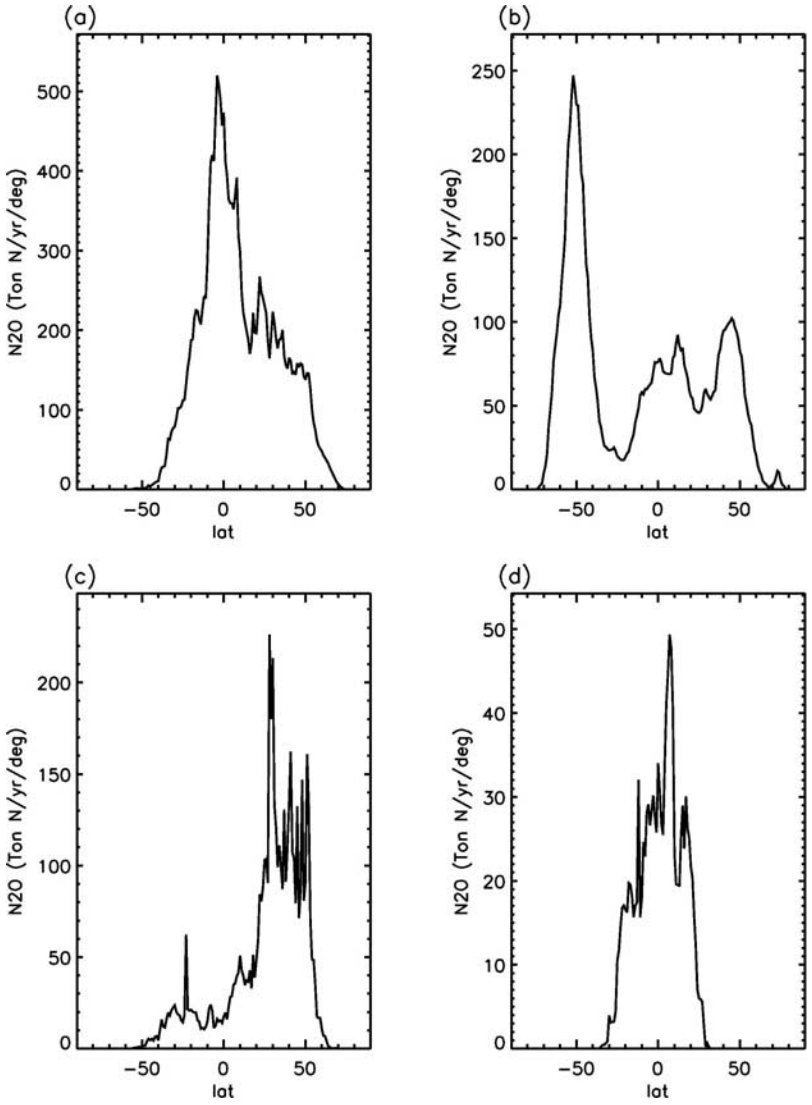

Figure 6. N_2O (Ton Nyr^{-1}) for the nine sources from GEIA. (a) Soil, (b) ocean, (c) sum of animal excreta, industry, fossil fuel burning, biofuel burning, and agriculture, and (d) sum of post–forest clearing soil and biomass burning.

partly due to the influence from the stratosphere [*Levin et al.*, 2002; *Liao et al.*, 2004; *Nevison et al.*, 2004]. Thus, from equation (4), we have

$$\frac{2A_1}{\omega\tau} = 0.5\,\text{ppb} \tag{5}$$

$$\frac{A_1}{\tau} = \frac{0.5\omega}{2} = 1.57\,\text{ppb/yr} = 7.54\,\text{TgN/yr}, \tag{6}$$

where we have used the conversion 1 ppb N_2O (global) equals 4.80 Tg N [see, e.g., *Morgan et al.*, 2004, section 4.7]. From Table 4, we have the steady state source $\frac{A_0}{\tau}$ = 13.55 TgN/yr. Combining this with equation (6), we arrive at the estimate, $\frac{A_1}{A_0}$ = 0.56. Therefore the seasonally varying part of the N_2O source is as much as 50% of the steady source.

4. Conclusion

[20] We have used the MTM spectrum analysis to derive a statistically significant seasonal cycle in the observed data from seven stations. Three stations are in the NH; two are in the SH and two in the tropics (see Table 2). The peak-to-peak amplitude of the N_2O seasonal cycle increases with latitude from 0.29 ppb at SPO to 1.15 ppb at ALT as shown in Figure 3a. There are also phase shifts in the maximum and minimum month of the seasonal cycles from the SH to

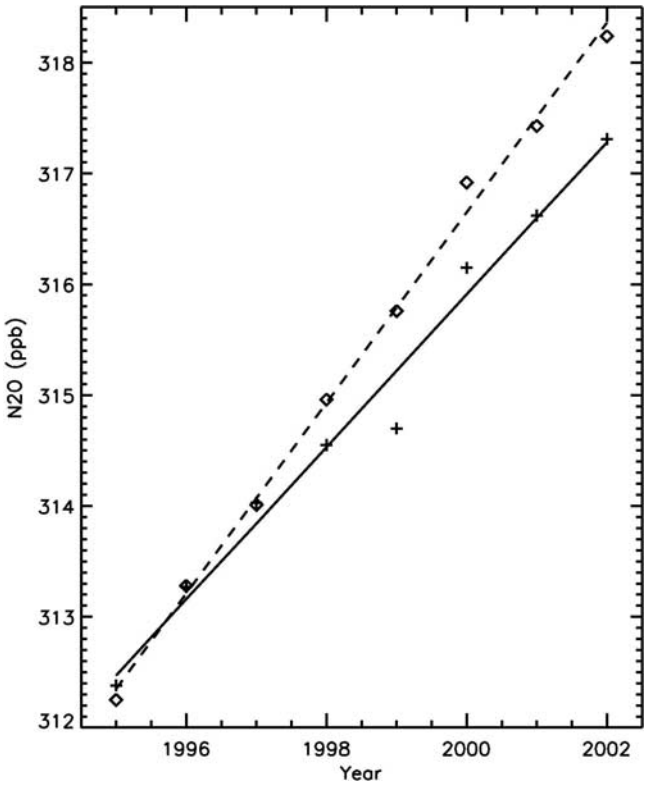

Figure 7. N_2O trend at Mace Head in June (solid line) and October (dashed line). Crosses and diamonds are the raw data for Mace Head in June and October, respectively.

NH. The trends in N_2O data are also seasonally dependent. The seasonal cycles of the N_2O trends at BRW, MHD, and SMO are larger than that at CGO.

[21] The N_2O seasonal cycle provides constraints for the N_2O surface sources. In the NH, the N_2O seasonal cycle may be influenced by the stratosphere. In the SH, the N_2O seasonal cycle may be mostly due to the ocean source. The N_2O seasonal cycle in the tropics is puzzling. We speculate that there is a much larger biomass burning and soil emission source for the tropics than in current models. Inverse modeling will be carried out to deduce the seasonal variability of the biological sources.

Appendix A: Estimation of Error in Computing the N_2O Seasonal Cycle

[22] The estimated errors for the weighted mean of multimeasurements are discussed in this appendix. We assume Gaussian distribution of measurement errors. In section A1, the standard deviation for the simplest case with only two measurements is discussed. In section A2, we extend the standard deviation for two-measurements to the multiple measurements case. Finally, we discuss the estimated errors for the N_2O measurements using the results from sections A1 and A2.

A1. Two-Measurement Case

[23] For a two-measurement case, the probability density function (PDF) can be written as

$$f_j(x_j) \propto \exp\left[-\left(x_j - \bar{x}_j\right)^2/\sigma_j^2\right], j = 1, 2 \ , \tag{A1}$$

where σ_j is the standard deviation for the measurement x_j. Thus the PDF for variable $x = x_1 + x_2$ is

$$\begin{aligned} f(x) \ &\propto \int_{-\infty}^{+\infty} f_2(x-t) f_1(t) dt \\ &\propto \int_{-\infty}^{+\infty} \exp\left[-(x - t - \bar{x}_2)^2/\sigma_2^2\right] \exp\left[-(t - \bar{x}_1)^2/\sigma_1^2\right] dt \\ &\propto \exp\left\{-[x - (\bar{x}_1 + \bar{x}_2)]^2/\left(\sigma_1^2 + \sigma_2^2\right)\right\}. \end{aligned} \tag{A2}$$

Therefore the mean of x is $\bar{x}_1 + \bar{x}_2$, and the standard deviation is $\sqrt{\sigma_1^2 + \sigma_2^2}$.

A2. Multimeasurement Case

[24] For multimeasurements $\{x_j\}$ with standard deviation $\{\sigma_j\}$, the PDF for variable $X = \sum_{j=1}^{N} x_j$ is

$$f(X) \propto \exp\left[-\left(X - \overline{X}\right)^2/\sigma_X^2\right], \tag{A3}$$

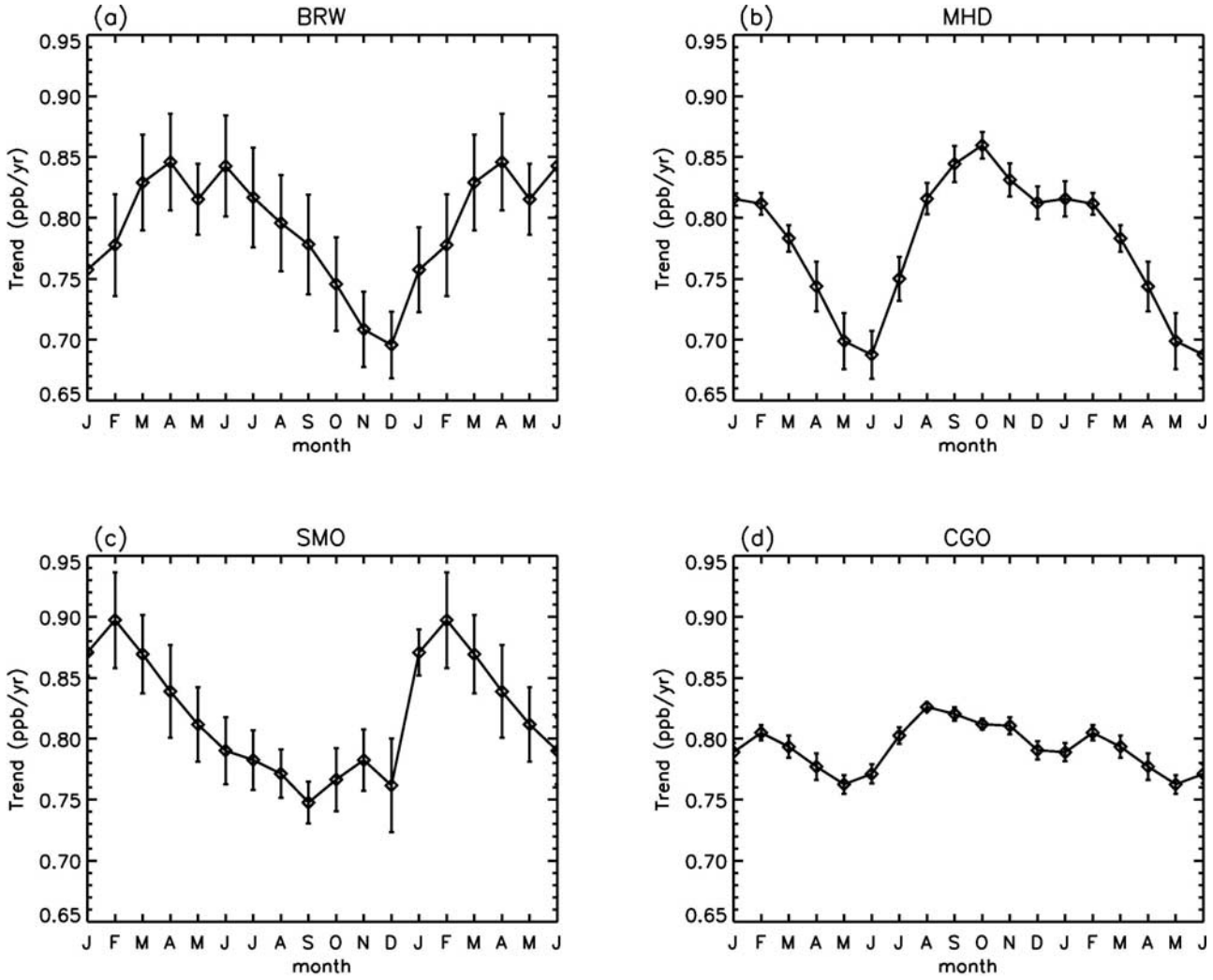

Figure 8. N_2O trend from the data of four stations. (a) Barrow, (b) Mace Head, (c) Cape Matatula, and (d) Cape Grim. The data for the first 6 months of the year are repeated after December.

where $\overline{X} = \sum_{j=1}^{N} \overline{x}_j$ and $\sigma_X = \sqrt{\sum_{j=1}^{N} \sigma_j^2}$. N is the total number of measurements.

[25] Thus the mean and the standard deviation for the variable $Y = \frac{1}{N} \sum_{j=1}^{N} x_j$ are separately $\overline{Y} = \frac{1}{N} \sum_{j=1}^{N} \overline{x}_j$ and $\sigma_Y = \frac{1}{N} \sqrt{\sum_{j=1}^{N} \sigma_j^2}$.

A3. N_2O-Measurement Case

[26] For the N_2O measurements $\{x_j\}$ discussed in paper, the monthly mean N_2O concentrations, $\overline{x}_j$, were measured with varying precision. Let σ_j represents the standard deviation for each measurement. We need consider the weighted value of the N_2O measurements, $Z = \sum_{j=1}^{N} (x_j/\sigma_j^2)\sigma_t^2$, where $\sigma_t^2 = \left[\sum_{j=1}^{N} 1/\sigma_j^2\right]^{-1}$ [*Liao et al.*, 2004]. From equation (A3), the PDF for variable Z can be written as

$$f(Z) \propto \exp\left[-(Z-\overline{Z})^2/\sigma_Z^2\right], \tag{A4}$$

where $\overline{Z} = \sum_{j=1}^{N} (\overline{x}_j/\sigma_j^2)\sigma_t^2$ and $\sigma_Z^2 = \sum_{j=1}^{N} (\sigma_t^2/\sigma_j^2)^2 \sigma_j^2 = \sigma_t^4 \sum_{j=1}^{N} (1/\sigma_j^2) = \sigma_t^2$.

[27] To further consider the N_2O variance due to the different seasonal values in different years, the standard deviation, σ, for the seasonal cycle of N_2O are finally determined by

$$\sigma = \sqrt{\sigma_Z^2 + \sigma_S^2}, \tag{A5}$$

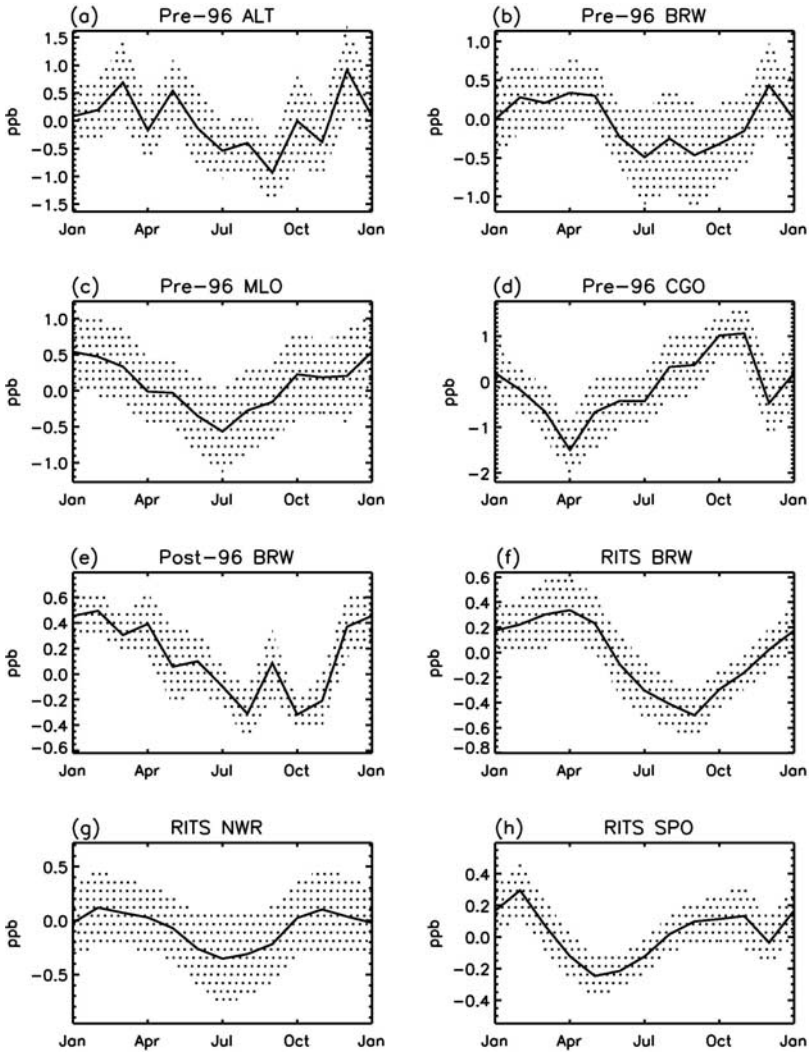

Figure B1. N_2O seasonal cycle (solid line) for the eight stations with large measurement errors. Shaded area represents the estimated error, $\sigma = \sqrt{\sigma_Z^2 + \sigma_S^2}$, for the seasonal cycle. (a) NOAA flask pre-1996 Alert, (b) NOAA flask pre-1996 Barrow, (c) NOAA flask pre-1996 Mauna Loa, (d) NOAA flask pre-1996 Cape Grim, (e) NOAA flask post-1996 Barrow, (f) RITS Barrow, (g) RITS Niwot Ridge (NWR), and (h) RITS South Pole.

where σ_Z^2 is the variance for the measurement errors, $\sigma_S^2 = \frac{1}{N}\sum_{j=1}^{N}(\bar{x}_j - x_j^*)^2$ is the variance for the seasonal values in each month, and x_j^* is the mean of $\bar{x}_j$ for a particular month over all years.

Appendix B: N_2O Seasonal Cycle in the Stations With Large Measurement Errors

[28] In Table 2, there are eight stations with significant seasonal cycles that are not used for detailed analysis in the main text. The measurement errors are relatively larger for these stations. For comparison purpose, we present their seasonal cycles in Figure B1. In the NH, there are six stations: NOAA flask pre-1996 Alert, NOAA flask pre-1996 Barrow, NOAA flask pre-1996 Mauna Loa, NOAA flask post-1996 Barrow, RITS Barrow, RITS Niwot Ridge (NWR). These six stations have positive values in winter and negative value in the summer. The maxima are before May ranging from 0.12 to 1.06 ppb. The minima are after June ranging from −1.49 to −0.24 ppb. In the SH, there are two stations: NOAA flask pre-1996 Cape Grim and RITS South Pole. They both have positive values before February and after August. NOAA flask pre-1996 Cape Grim has maximum of 1.1 pb in November, while the minimum is −1.5 ppb in April. RITS South Pole has a maximum of 0.29 ppb in February and a minimum about −0.25 ppb in May. When we include the seasonal cycles from NWR and MLO in Figure 4, then we obtain Figure B2. Since the positions of MLO and KUM are very close, we average the seasonal cycles from these two stations. There is some discontinuity for the N_2O seasonal cycle in the NH due to result from station NWR. However, considering the large error bars, these results are still consistent with those for the

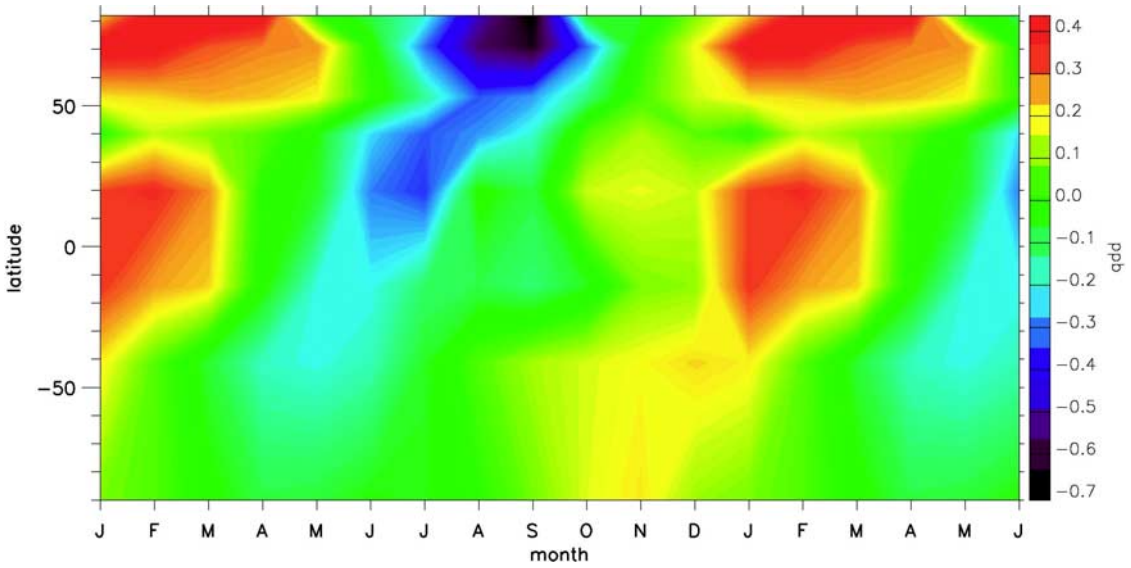

Figure B2. Seasonal cycle from data for nine stations: Alert, Barrow, Cape Kumukahi, Mace Head, Niwot Ridge, Mauna Loa, Cape Matatula, Cape Grim, and South Pole. The data for the first 6 months of the year are repeated after December.

seven stations summarized in Figure 1d and Figure 2. With precise and high-quality data available in the future, we should be able to obtain a better seasonal cycle of N_2O.

[29] **Acknowledgments.** We thank T. Liao for the helpful discussions and two anonymous reviewers for helpful comments. We also want to acknowledge J. H. Butler, G. S. Dutton, and T. M. Thompson for providing their individual data sets from NOAA. We would like to acknowledge our colleagues from the AGAGE network for providing their in situ sampling data through the web and for collecting NOAA flasks at their stations (CGO, MHD). This research was supported in part by NSF grant ATM-9903790. Yuk L. Yung acknowledges support by the Davidow Fund.

References

Battle, M., et al. (1996), Atmospheric gas concentrations over the past century measured in air from firn at the South Pole, *Nature*, *383*, 231–235.

Bouwman, A. F., K. W. van der Hoek, and J. G. J. Oliver (1995), Testing high-resolution nitrous oxide emission estimates against observations using an atmospheric transport model, *J. Geophys. Res.*, *100*, 2785–2800.

Camp, C. D., M. S. Roulston, A. F. C. Haldemann, and Y. L. Yung (2001), The sensitivity of tropospheric methane to the interannual variability in stratospheric ozone, *Chemosphere Global Change Sci.*, *3*, 147–156.

Cicerone, R. (1989), Analysis of sources and sinks of atmospheric nitrous oxide (N_2O), *J. Geophys. Res.*, *94*, 18,265–18,271.

Ghil, M., et al. (2002), Advanced spectral methods for climatic time series, *Rev. Geophys.*, *40*(1), 1003, doi:10.1029/2000RG000092.

Levin, I., et al. (2002), Three years of trace gas observations over the Euro-Siberian domain derived from aircraft sampling—A concerted action, *Tellus, Ser. B*, *54*, 696–712.

Liao, T., C. D. Camp, and Y. L. Yung (2004), The seasonal cycle of N_2O, *Geophys. Res. Lett.*, *31*, L17108, doi:10.1029/2004GL020345.

McElroy, M. B., S. C. Wofsy, and Y. L. Yung (1977), Nitrogen cycle—Perturbations due to man and their impact on atmospheric N_2O and O_3, *Philos. Trans. R. Soc., Ser. B*, *277*, 159–181.

McLinden, C. A., M. J. Prather, and M. S. Johnson (2003), Global modeling of the isotopic analogues of N_2O: Stratospheric distributions, budgets, and the ^{17}O–^{18}O mass-independent anomaly, *J. Geophys. Res.*, *108*(D8), 4233, doi:10.1029/2002JD002560.

Minschwaner, K., R. J. Salawitch, and M. B. McElroy (1993), Absorption of solar-radiation by O_2–Implications for O_3 and lifetimes of N_2O, $CFCL_3$, and CF_2CL_2, *J. Geophys. Res.*, *98*(D6), 10,543–10,561.

Morgan, C. G., M. Allen, M. C. Liang, R. L. Shia, G. A. Blake, and Y. L. Yung (2004), Isotopic fractionation of nitrous oxide in the stratosphere: Comparison between model and observations, *J. Geophys. Res.*, *109*, D04305, doi:10.1029/2003JD003402.

Nevison, C. D., D. E. Kinnison, and R. F. Weiss (2004), Stratospheric influences on the tropospheric seasonal cycles of nitrous oxide and chlorofluorocarbons, *Geophys. Res. Lett.*, *31*, L20103, doi:10.1029/2004GL020398.

Nevison, C. D., R. F. Keeling, R. F. Weiss, B. N. Popp, X. Jin, P. J. Fraser, L. W. Porter, and P. G. Hess (2005), Southern Ocean ventilation inferred from seasonal cycles of atmospheric N_2O and O_2/N_2 at Cape Grim, Tasmania, *Tellus, Ser. B*, *57*, 218–229.

Prinn, R. G., et al. (1990), Atmospheric emissions and trends of nitrous oxide deduced from 10 years of ALE-GAGE data, *J. Geophys. Res.*, *95*, 18,369–18,385.

Prinn, R. G., et al. (2000), A history of chemically and radiatively important gases in air deduced from ALE/GAGE/AGAGE, *J. Geophys. Res.*, *105*, 17,751–17,792.

Stein, L. Y., and Y. L. Yung (2003), Production, isotropic composition, and atmospheric fate of biologically produced nitrous oxide, *Annu. Rev. Earth Planet. Sci.*, *31*, 329–356.

Thompson, T. M., et al. (2004), Halocarbons and other atmospheric trace species, *Summary Rep. 27 2002–2003*, edited by R. C. Schnell et al., pp. 115–135, Clim. Monit. Diagn. Lab., U.S. Dep. of Commer., Boulder, Colo.

Volk, C. M., J. W. Elkins, D. W. Fahey, G. S. Dutton, J. M. Gilligan, M. Loewenstein, J. R. Podolske, K. R. Chan, and M. R. Gunson (1997), Evaluation of source gas lifetime from stratospheric observations, *J. Geophys. Res.*, *102*, 25,543–25,564.

J. W. Elkins, Earth System Research Laboratory, Global Monitoring Division, NOAA, 325 Broadway, Boulder, CO 80305-3328, USA. (james.w.elkins@noaa.gov)

X. Jiang, Division of Geological and Planetary Sciences, California Institute of Technology, Pasadena, CA 91125, USA. (xun@gps.caltech.edu)

W. L. Ku, Department of Physics, Chinese University of Hong Kong, Shatin, New Territories, Hong Kong. (kwl@gps.caltech.edu)

Q. Li, Jet Propulsion Laboratory, M/S 183-501, California Institute of Technology, 4800 Oak Grove Drive, Pasadena, CA 91109, USA. (qinbin.li@jpl.nasa.gov)

R. G. Prinn, Center for Global Change Science, Department of Earth, Atmospheric, and Planetary Science, Massachusetts Institute of Technology, 77 Massachusetts Avenue, Cambridge, MA 02139-4307, USA. (rprinn@mit.edu)

R.-L. Shia and Y. L. Yung, Division of Geological and Planetary Sciences, California Institute of Technology, Pasadena, CA 91125, USA. (rls@gps.caltech.edu; yly@gps.caltech.edu)